Inorganic Chemistry

Article

pubs.acs.org/IC

Photo- and Thermochromic and Adsorption Properties of Porous Coordination Polymers Based on Bipyridinium Carboxylate Ligands

Oksana Toma,[†] Nicolas Mercier,*[,†] Magali Allain,[†] Abdel Adi Kassiba,[γ] Jean-Pierre Bellat,[§] Guy Weber,[§] and Igor Bezverkhyy[§]

[†]MOLTECH Anjou, UMR-CNRS 6200, Université d'Angers, 2 Bd Lavoisier, 49045 Angers, France

[γ]IMMM, UMR-CNRS 6283, Université du Maine, Avenue O. Messiaen, 72085 Le Mans, France

[§]ICB, UMR-CNRS 6303, Université de Bourgogne, 9 A. Savary, 21078 Dijon, France

Supporting Information

ABSTRACT: The zwitterionic bipyridinium carboxylate ligand 1-(4-carboxyphenyl)-4,4′-bipyridinium (hpc1) in the presence of 1,4-benzenedicarboxylate anions (BDC^{2-}) and Zn^{2+} ions affords three porous coordination polymers (PCPs): $[Zn_5(hpc1)_2(BDC)_4(HCO_2)_2]\cdot 2DMF\cdot EtOH\cdot H_2O$ (**1**), $[Zn_3(hpc1)(BDC)_2(HCO_2)(OH)(H_2O)]\cdot DMF\cdot EtOH\cdot H_2O$ (**2**), and $[Zn_{10}(hpc1)_4(BDC)_7(HCO_2)_2(OH)_4(EtOH)_2]\cdot 3DMF\cdot 3H_2O$ (**3**), with the formate anions resulting from the in situ decomposition of dimethylformamide (DMF) solvent molecules. **1** and **3** are photo- and thermochromic, turning dark green as a result of the formation of bipyridinium radicals, as shown by electron paramagnetic resonance measurements. Particularly, crystals of **3** are very photosensitive, giving an eye-detectable color change upon exposure to the light of the microscope in air within 1−2 min. A very nice and interesting feature is the regular discoloration of crystals from the "edge" to the "core" upon exposition to O_2 (reoxidation of organic radicals) due to the diffusion of O_2 inside the pores, with this discoloration being slower in an oxygen-poor atmosphere. The formation of organic radicals is explained by an electron transfer from the oxygen atoms of the carboxylate groups to pyridinium cycles. In the structure of **3′**, $[Zn_{10}(hpc1)_4(BDC)_7(OH)_6(H_2O)_2]$, resulting from the heating of sample **3** (desolvation and loss of CO molecules due to the decomposition of formate anions), no suitable donor−acceptor interaction is present, and as a consequence, this compound does not exhibit any chromic properties. The presence of permanent porosity in desolvated **1**, **2**, and **3′** is confirmed by methanol adsorption at 25 °C with the adsorbed amount reaching 5 wt % for **1**, 10 wt % for **3′**, and 13 wt % for **2**. The incomplete desorption of methanol at 25 °C under vacuum points to strong host−guest interactions.

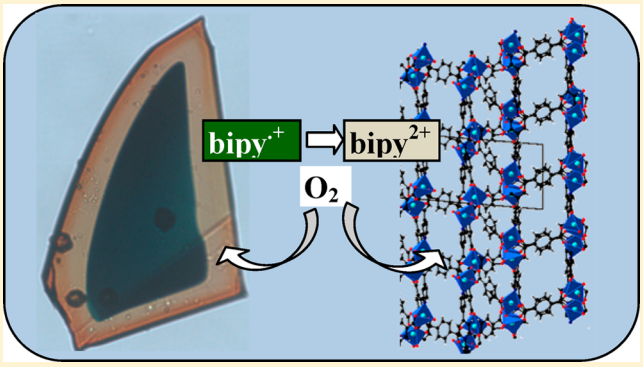

1. INTRODUCTION

In the field of porous coordination polymers (PCPs) or metal−organic frameworks (MOFs),[1] a great tendency is the use of functional ligands, which, in addition to their structural role in the building of frameworks through their neutral or anionic chelating sites, have abilities through their core to make interactions with guest molecules. Most of the ligands' cores are neutral, while a few are cationic. In fact, the presence of cationic sites on ligands adds a difficulty to building porous compounds because of the great tendency of interactions with electron-rich sites such as carboxylate groups, precluding the formation of pores. However, this strategy of using cationic ligands has been considered quite recently in the context of the importance of a high concentration of accessible cationic sites for the efficiency of H_2[2] or CO_2[3] (precombustion process) uptake. This has mainly been achieved through the metal at the nodes of networks, which becomes "metal open site" after departure of initially binding solvent molecules,[4] but also by using metal complexes of porphyrin type as ligands[5] or by incorporating small cations as Li^+ through postsynthetic reactions.[6] Finally, a few PCPs with cationic linkers have been reported quite recently, based on bipyridinium parts[7−10] or imidazolium moieties.[11] Bipyridiniums, also called viologens (V^{2+}), besides its cationic character, are a well-known class of electron-acceptor redox units that undergo two reversible, one-electron reductions.[12] The applications in chemistry of viologens mainly take advantage of the first reversible reduction step involving $V^{2+}/V^{\bullet+}$ and of the color changes during the first reduction step due to the different absorption domains of V^{2+} (UV) and $V^{\bullet+}$ (visible). In the solid state, materials incorporating bipyridinium units can undergo a direct charge-transfer process in the case of good electron-donor partners[12,13] or a photoinduced charge-transfer (PICT) process in the case of worse electron-donor partners such as chlorides[14,15] or carboxylates. Zhang's group has reported most of the coordination polymer (CP)

Received: April 30, 2015
Published: September 10, 2015

DOI: 10.1021/acs.inorgchem.5b00975
Inorg. Chem. 2015, 54, 8923−8930

materials based on "bipyridinium carboxylate" ligands, where the carboxylate bearing unit is anchored to the bipyridinium core.[16−21] These dense compounds can be photochromic and sometimes thermochromic because of a PICT process from an oxygen atom of the carboxylate groups to the nitrogen atom of pyridinium cycles. Recently, an interesting compound exhibiting photochromism and luminescence pH sensing due to protonation of the pyridyl groups of bipyridinium units was reported.[22] In contrast, PCPs based on such ligands are scarce. To the best of our knowledge, only a few compounds have been reported by Kitagawa et al.[7] and Zhang et al.[8] They showed that the pyridinium cationic surface participates in the strong adsorption of methanol (MeOH)[7] or can selectively accommodate aromatic donors such as hydroquinone.[8a] Some other materials, either containing anions in pores[9] or based on 1D CPs or complexes including solvent molecules,[10] have been reported more recently. In the field of chemical sensors, despite the growing catalogue of PCP materials, the goal of highly selective recognition and high dynamic adsorption, which are key parameters for applications, remains unrealized for most analytes.[23] For most PCPs, the high level of specificity can be achieved by shape or size selectivity only (molecular sieving). The design of PCPs having the possibility of inducing chemically specific interactions between guests and the internal surface of pores, as a source of selectivity and of a dynamic adsorption medium,[24−27] is of great interest. Thus, PCPs with walls based on bipyridinium units have great potential for the detection of electron-rich molecules or those having permanent dipolar moments, such as NH_3, SO_2, HCOH, MeOH, etc.

In this context, we report on three new PCPs based on bipyridinium carboxylate ligands in the Zn^{2+}/BDC^{2-}/hpc1 system (BDC^{2-} = 1,4-benzenedicarboxylate and hpc1 = 1-(4-carboxyphenyl)-4,4′-bipyridinium; see Scheme 1):

Scheme 1. Structural Formulas of Ligands Used in This Work

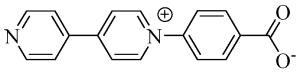

1-(4-carboxyphenyl)-4,4'-bipyridinium (***hpc1***)

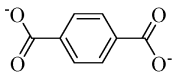

1,4-benzene-dicarboxylate ($\mathbf{BDC^{2-}}$)

$[Zn_5(hpc1)_2(BDC)_4(HCO_2)_2]\cdot 2DMF\cdot EtOH\cdot H_2O$ (**1**), $[Zn_3(hpc1)(BDC)_2(HCO_2)(OH)(H_2O)]\cdot DMF\cdot EtOH\cdot H_2O$ (**2**), and $[Zn_{10}(hpc1)_4(BDC)_7(HCO_2)_2(OH)_4(EtOH)_2]\cdot 3DMF\cdot 3H_2O$ (**3**). Upon heating, a decarboxylation also occurs for crystals of **3**, leading to the compound whose host network is $[Zn_{10}(hpc1)_4(BDC)_7(OH)_6(H_2O)_2]$ (**3′**).We will show that these materials, which adsorb MeOH, display impressive photo- and thermochromic properties with a particular highlight on the clear discoloration of crystals of **3** from the edges to the core as a result of oxidation of the bipyridinium radicals by O_2.

2. EXPERIMENTAL SECTION

2.1. Synthesis and Characterization. Compounds **1**−**3** were synthesized by a solvothermal method, by the reaction of $Zn(NO_3)_2\cdot 6H_2O$ with terephthalic acid (H_2BDC) and 1-(4-carboxyphenyl)-4,4′-bipyridinium chloride (Hhpc1)·Cl in a mixture of solvents [dimethylformamide (DMF), ethanol (EtOH), and water (H_2O)]. The three compounds were obtained from the same stoichiometry of the starting reagents but under different heating programs and with different ratios of the solvent mixture (see the Supporting Information, SI). They all contain the HCO_2^- anions, which result from the hydrolysis of DMF molecules during the synthesis. Light-brown crystals of **1**, small orange/brown needles of **2**, and yellow/brown platelike crystals of **3** were filtered off and washed with EtOH. It must be noted that crystals of **2** are always obtained with a number of crystals of **1** (approximately with a ratio of 80/20 for **2**/**1**). However, a selection of crystals of **2** under the microscope has allowed powder X-ray diffraction (PXRD), thermogravimetric analysis (TGA), and elemental analyses.

PXRD patterns of **1**−**3** using a D8 Bruker diffractometer (Cu $K\alpha_{1,2}$ radiation) equipped with a linear Vantec super speed detector, have shown that all of the observed reflections could be indexed in the unit cell parameters obtained from single-crystal X-ray diffraction experiments (see the SI). The UV−vis absorption spectra of the solid-state samples were recorded on a PerkinElmer Lambda 950 spectrometer, equipped with an integrating sphere in the 250−900 nm range.

TGA of **1**−**3** was performed on a TGA-2050 analyzer from TA Instruments in the range of 20−800 °C (see the SI). They all reveal a two-step desolvation: the first step corresponding to the departure of H_2O or EtOH molecules and the second step at higher temperature (T = 170 °C) corresponding, as expected, to the release of DMF molecules. In the TGA curve of **1**, the first weight loss of 3.62% is assigned to the departure of one H_2O molecule and one EtOH molecule per formula unit (calcd 3.48%), while the second weight loss of 7.46% can be assigned to the removal of two DMF molecules (calcd 7.95%). In the TGA curve of **2**, the theoretical weight loss of 13.45% (one H_2O, one EtOH, and one DMF per formula unit) well corresponds to the experimental total weight loss of 13.55%. The first step from 25 to 260 °C (6.62%) can be assigned to the loss of EtOH and H_2O molecules (calcd 6.28%), while the second step of 6.93% corresponds to the release of DMF molecules (calcd 7.17%). In the TGA curve of **3**, the first step of 3.81% is assigned to the loss of two EtOH and three H_2O molecules per formula unit (calcd 3.73%), while the second step (weight loss of 8.07%) is assigned to the loss of three DMF and two CO groups (calcd 8.01%), resulting from decomposition of the formate anion, as shown by single-crystal analysis (see the text). The hypothesis on the nature and quantity of solvent molecules deduced from X-ray analysis and TGA is in quite good accordance with the result of elemental analysis. **1**. Exptl: C, 49.37; H, 3.61; N, 4.35; O, 24.15. Calcd: C, 49.70; H, 3.48; N, 4.57; O, 24.38. **2**. Exptl C, 45.77; H, 3.43; N, 3.87; O, 27.13. Calcd: C, 46.02; H, 3.83; N, 4.13; O, 26.70. **3**. Exptl: C, 48.21; H, 3.26; N, 4.27; O, 25.19. Calcd: C, 48.65; H, 3.52; N, 4.49; O, 24.23.

2.2. X-ray Crystallography. X-ray diffraction data were collected on a Bruker-Nonius Kappa CDD diffractometer equipped with a graphite-monochromated Mo Kα radiation (λ = 0.71073 Å; **1**, **3**, and **3′**) and on an Agilent SuperNova diffractometer equipped with an Atlas CCD detector using mirror-monochromated microfocus Cu Kα radiation (λ = 1.54184 Å; **2**). Crystals of **3′** have been obtained by the slow heating of crystals of **3** up to 200 °C. After cooling to room temperature, the crystals were kept in air for a few hours before data collection at 150 K of a selected crystal, explaining the presence of H_2O in **3′**, both in pores and coordinated to zinc ions (see the SI). A summary of crystallographic data and refinement results for the four structures (**1**−**3** and **3′**) is listed in Table 1. Structures were solved and refined using the *Shelxl97* package. Positions and atomic displacement parameters were refined by full-matrix least-squares routines against F^2. All hydrogen atoms were treated with a riding model. Except for EtOH in **2**, the solvent molecules in pores were not located, but the corresponding scattering contribution was taken into account using a *SQUEEZE/PLATON* procedure (see the CIF files). CCDC 1061551−1061554 are for **3′** and **1**−**3**, respectively.

Finally, refinements of the positions of all non-hydrogen atoms and of anisotropic displacement parameters lead to R = 0.051, 0.076, 0.055, and 0.061 for **1**−**3** and **3′**, respectively. A complete list of crystallographic data, along with the atomic coordinates, anisotropic

DOI: 10.1021/acs.inorgchem.5b00975
Inorg. Chem. 2015, 54, 8923−8930

Table 1. Crystallographic Data for 1−3 and 3′

	1	2	3	3′
fw (g mol^{-1})	1836.18	1017,84	3431.17	3225.87
T (K)	293	120	150	150
space group	$P\bar{1}$	$P2_1/c$	$P\bar{1}$	$P\bar{1}$
a (Å)	9.8071(5)	11.497(1)	11.092(1)	11.478(1)
b (Å)	11.615(1)	33.542(3)	12.199(2)	12.377(1)
c (Å)	16.544(2)	12.106(1)	28.767(5)	25.794(3)
α (deg)	103.75(1)	90	97.64(1)	80.25(1)
β (deg)	104.54(1)	116.84(1)	92.01(1)	88.09(1)
γ (deg)	95.91(1)	90	115.94(1)	65.25(1)
V (Å^3)	1745.3(2)	4165.6(7)	3450.4(9)	3277.0(5)
Z	1	4	1	1
obsd reflns [$I > 2\sigma(I)$] [R_{int}]	8393 [0.054]	15727 [0.051]	15266 [0.036]	13807 [0.045]
no. of param	457	514	948	879
R1 [$I > 2\sigma(I)$]/ wR2 (all data)	0.051/0.136	0.076/0.177	0.055/0.15	0.061/0.177

displacement parameters, and bond distances and angles for each compound, is given as CIF files.

2.3. Electron Paramagnetic Resonance (EPR). EPR experiments were performed with a Bruker EMX spectrometer using an X-band microwave bridge (9.5 GHz) and a variable-temperature Bruker Unit ER 4111 VT working in the range of 170−500 K with good stabilization (±0.1 K). The experiments were carried out by using a low modulation field (3 G) and 200 mW as the microwave power. These parameters are suitable for recording the EPR spectra without any distortion. Numerical simulations of the EPR spectra were performed by using the commercial Bruker *WinSimfonia* software, leading to the magnetic **g**-tensor components of the EPR-active centers and the features of the resonance line shape related to the dynamics of the centers and their mutual interactions. As expected from the structure of the bipyridinium radicals, the presence of a hyperfine structure induced by the nitrogen nuclei interacting with the unpaired electrons can also be accounted for from the EPR line-shape features.

2.4. Adsorption Measurements. Adsorption−desorption isotherms of MeOH on **1** and **3** were measured at 25 °C using a home-built McBain-type thermobalance. Before measurements, the samples (ca. 15 mg) were outgassed at 180 °C under vacuum (10^{-6} hPa) overnight. Then, measurement of the adsorption branch of the isotherms was started by introducing MeOH into the balance, with the pressure increasing incrementally from 0.1 to about 150 hPa (the saturation MeOH pressure at 25 °C was equal to 162 hPa). After the introduction of each dose of MeOH, the sample weight was measured continuously until its stabilization. The values of the pressure and weight gain at each equilibrium state were used to construct the adsorption isotherm. Once the highest pressure value had been attained, the desorption branch of the isotherm was measured by progressively decreasing the MeOH pressure. The estimated experimental error on the adsorbed amount was about 1 mg g^{-1}. The accuracy of the pressure measurement was 1%, and the temperature was maintained within 1 °C.

3. RESULTS AND DISCUSSION

3.1. Structure and Photochromism of 1. The asymmetric unit of **1** involves three Zn^{2+} ions (two in general positions and one in a special position with an occupancy of 0.5), two BDC^{2-} molecules, one hpc1 unit, and one HCO_2^-. The three Zn^{2+} ions are hexa- (ZnO_6), penta- (ZnO_4N), and tetracoordinated (ZnO_4), and they form two types of clusters. The first cluster is made by two equivalent pentacoordinated zinc atoms, connected to each other by the oxygen atoms of four BDC^{2-} molecules, forming a so-called paddle-wheel cluster, with the apical position being occupied by the nitrogen atoms of hpc1 molecules (Figure 1a). The second type of

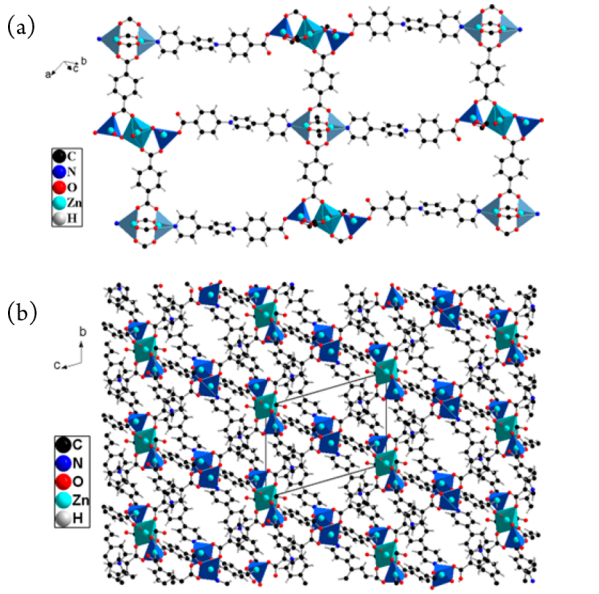

Figure 1. Structure of **1**: one 3D network showing the two kinds of nodes (di- and trinuclear) (a) and a general view of the structure resulting from the interpenetration of three 3D networks (b).

cluster includes two tetrahedral and one hexacoordinated zinc atoms linked by four bidentate BDC^{2-} dianions (as in the previous case), two oxygen atoms of two monodentate formate groups, and two hpc1 molecules bonded to the tetracoordinated Zn^{2+} ions through the oxygen atoms of the carboxylate sides. The two kinds of clusters together with the connectors, hpc1 and BDC^{2-} molecules, define a 3D network: each node, dinuclear or trinuclear, is connected along the b axis to two nodes of the other type of cluster through the hpc1 molecules, while each node is also connected in perpendicular directions to four nodes of the other nature through BDC^{2-} dianions (Figure 1a). The resulting structure comes from the interpenetration of three such 3D networks (Figure 1b). It is worth noting that solvent molecules inside the pores were not defined by X-ray analysis. The *SQUEEZE* routine of *PLATON* gives 14% per unit volume of potential void space. The TGA experiment shows that desolvation occurs in the 50−200 °C range, while the desolvated compound is stable up to 300 °C. PXRD measurements along with the temperature (thermodiffractometry) have been performed, showing no significant change in the peak positions up to 250 °C. This reveals the robustness of the network, without any breathing or great modification upon desolvation. At 260 °C, a loss of crystallinity was observed (see the SI).

Interestingly, **1** possesses thermo- and photochromic properties and undergoes a net color change from yellow to dark green upon continuous irradiation with a UV lamp in air at room temperature or when heated at 240 °C for 10 min. The dark-green color of the crystals, which are kept up in an inert atmosphere in the dark (or under vacuum), is unchanged, but its initial color turns within a few hours in the presence of air. The development and fading of the color can be repeated many times without a noticeable loss (reversible character). This particularly shows that the solvent, initially present in the pores,

DOI: 10.1021/acs.inorgchem.5b00975
Inorg. Chem. 2015, 54, 8923−8930

does not seem to have an important role because it is removed after the first cycle at 250 °C. After irradiation of the sample upon UV irradiation, strong absorption bands appear on the UV−vis spectrum, centered at 635 and 715 nm, which are characteristic of viologen radicals (Figure 2). This suggests that

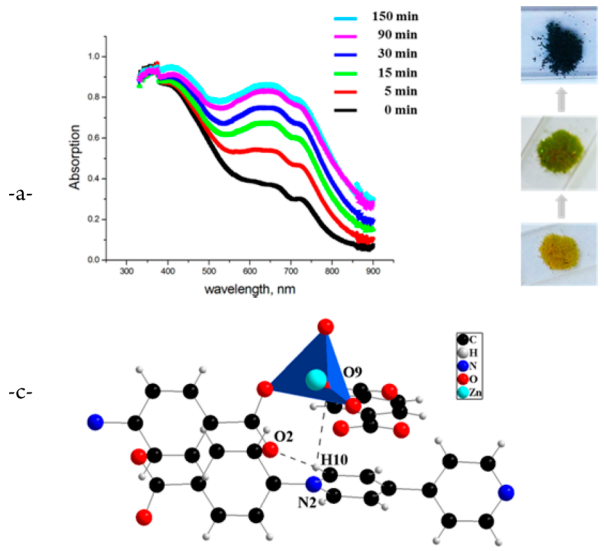

Figure 2. UV−vis spectra of irradiated crystals of **1** (a), photographs of crystals before and after irradiation (b), and detail of the structure showing short contacts involving the bipyridinium unit (c).

the color change of **1** arises from generation of the bipyridinium radicals, as a result of a photoreduction process. The observed discoloration is very certainly related to the oxidation process of the hpc1 radicals by O_2 from air because it has been observed in such photochromic compounds. Analysis of the interactions involving bipyridinium cycles does not reveal known favorable geometrical parameters, which are a short distance between the donor and the nitrogen atom of the pyridinium cycle and an angle between the donor−N^+ line and the normal of the pyridinium plane (δ) close to 0°.[14] Thus, in **1**, the oxygen atom O9 from a COO^- group is quite far from N^+ [d(N2···O9) = 3.87 Å], and above all, the δ angle is of 40.8°. However, we notice a short contact between the hydrogen atom bearing the carbon atom in the α position of N^+ and the oxygen atom O2 [d(O2···H10) = 2.30 Å], with this atom being coplanar with the pyridinium ring (Figure 2c). Such a situation could be a favorable pathway for the PICT process.

3.2. Structures of 2 and 3 and Photochromism of 3. The structures of the $[Zn_3(hpc1)(BDC)_2(HCO_2)(OH)(H_2O)]\cdot DMF\cdot EtOH\cdot H_2O$ (**2**) and $[Zn_{10}(hpc1)_4(BDC)_7(HCO_2)_2(OH)_4(EtOH)_2]\cdot 3DMF\cdot 3H_2O$ (**3**) compounds are quite similar. In fact, both of them are based on trinuclear clusters, containing three independent tetra- (ZnO_4), penta- (ZnO_5), and hexacoordinated (ZnO_5N) Zn^{2+} ions with one OH^- group binding the three cations (Figure 3a). These trinuclear units are surrounded by four BDC^{2-}, two hpc1, one HCO_2^-, and one H_2O molecule (**2**) or one EtOH molecule (**3**). In the structure of **2**, the OH^- group is interacting with the oxygen atom of a disordered EtOH molecule with a (O)H···O(EtOH) contact of 1.899(2) Å [d(O(H)···O(EtOH) = 2.690(2) Å; Figure 3b]. In **3**, the same kind of OH···O interaction is found, but the oxygen atom belongs to a H_2O molecule. In the structure of **3**, another binuclear building block of two hexacoordinated Zn^{2+} atoms

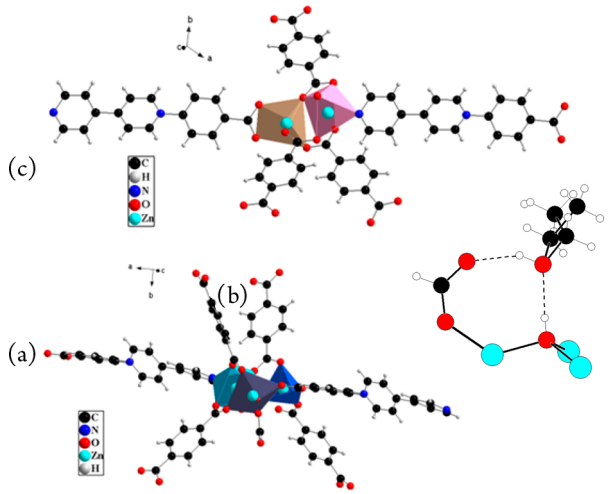

Figure 3. (a) Trinuclear building block found in the structures of **2** and **3**. (b) Interactions involving the OH^- linked to three Zn^{2+} ions, the free disordered EtOH molecule, and one formate anion in the structure of **2**. (c) Dinuclear building block found in the structure of **3**.

(ZnO_6 and ZnO_5N), linked together by three oxygen atoms of two BDC^{2-} groups, is found. Finally, the Zn^{2+} cations are surrounded by three BDC^{2-} anions, two hpc1 molecules (bonded by the *N*-pyridyl and COO^- sides, respectively), one HCO_2^-, which bridges the two kinds of clusters, and a OH^- group (Figure 3c). In both structures, the CPs are extended in the three directions, resulting in porous networks whose potential void spaces have been estimated to 22% and 14% per unit volume using the *SQUEEZE* routine of *PLATON* for **2** and **3**, respectively. The overall structures are displayed in Figure 4. Channels along one direction of the structures are well-defined with two kinds of windows in the structure of **3**, while only one is present in the structure of **2**. The aperture of the largest windows has been estimated to 5 × 5 $Å^2$. Upon heating, as indicated by powder X-ray thermodiffractometry measurements, a significant change of the peak positions in the pattern of **3** occurs (see the SI). This feature often reveals a breathing effect upon removal of the solvent molecules. However, in **3**, in addition to the departure of solvent molecules of DMF during the second weight loss step, CO molecules resulting from decomposition of the formate anions (into OH^- and CO) bridging the two kinds of clusters in **3**, are also removed. This is clearly demonstrated by a single-crystal X-ray study of slowly heated crystals of **3**, which, fortunately, partially retain their crystalline character through the phase transition, leading to **3′**. On the one hand, formate decomposition leads to, condensation of the two kinds of clusters into a pentameric unit in the structure of **3′**; on the other hand, a partial closing of one kind or pore is observed (Figure 4c).

Crystals of **3** are very photosensitive, giving an eye-detectable color change upon exposure to the light of the microscope in air within 1−2 min (Figure 5a). Crystals turn from light brown to dark green, and this change is a sign that a PICT process has occurred, leading to the appearance of hpc1 radicals (see the EPR spectrum in the SI). The return to the initial color is achieved after a few hours in the presence of air. This phenomenon has a reversible character, and even after more than 20 cycles, no degradation or decrease of the efficiency in the color change of the crystals was observed. Crystals of **3** are also thermochromic. We discovered this phenomenon by heating irradiated crystals in order to check, as is known, that

DOI: 10.1021/acs.inorgchem.5b00975
Inorg. Chem. 2015, 54, 8923−8930

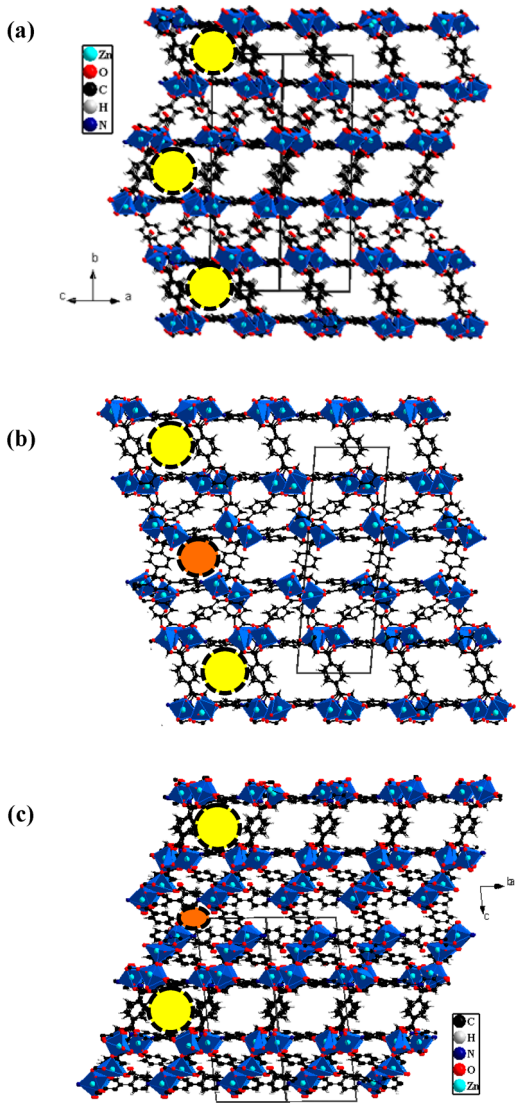

Figure 4. General view of the structures of **2** (a), **3** (b), and **3′** (desolvated **3**) (c) showing the kinds of pores (one in **2** and two in **3**) and the reduction of one type of pore correlated to the decreasing of the *c* parameter in **3′** as a result of decomposition of the formate anions upon heating.

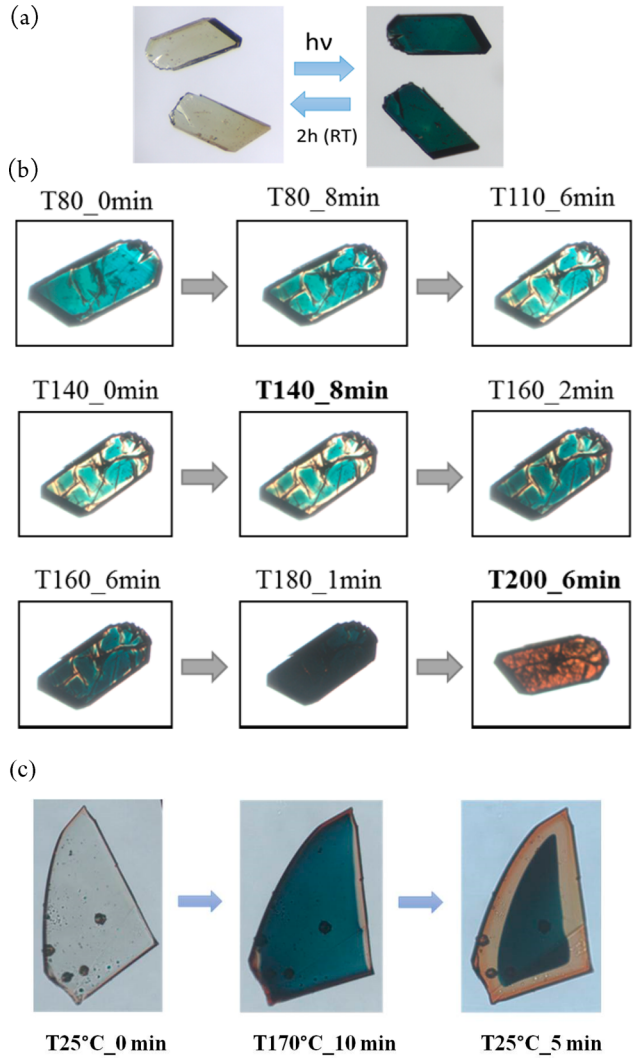

Figure 5. Photo- and thermochromism of crystals of **3**: color change after 1 or 2 min of irradiation upon a microscope light (a); behavior of one previously irradiated crystal along with the temperature (b); discoloration of a crystal from the edge to the core (c).

the time necessary to recover the initial color is strongly decreased at higher temperature. Figure 5b illustrates the thermal behavior of one previously irradiated crystal. Up to 140 °C, an expected discoloration of the crystal was observed but only at the interface of their fracture lines. The break of the crystal certainly results from the departure of solvent molecules, corresponding to the first step of weight loss on the TGA curve. Interestingly, when the temperature increases up to 160 °C, the green color starts to be restored, and the crystal becomes completely green at 180 °C. The heating of nonirradiated crystals confirmed that the beginning of the color change was approximately 140 °C and the maximal deep-dark-green color was reached at 160−180 °C. However, if the temperature is held for a long time in the 160−180 °C range, a temperature range that corresponds to the beginning of the second weight loss in the TGA curve, or if it goes over 200 °C, the green crystals become orange (Figure 5b). Besides the release of DMF molecules, the X-ray study of a single crystal slowly heated at 200 °C will show that CO molecules are also removed as a result of decomposition of the bridging formate anions, leading to structural changes (see below).

This evolution, from yellow-brown (initial color) to green (heated crystals up to 180 °C) and finally to orange (heating over 180 °C), revealing the appearance and disappearance of bipyridinium radicals, has been confirmed by EPR measurements (Figure 6). The intensity of the EPR signal starts to grow from 140 °C, indicating the formation of organic radicals ($g_{x,y,z}$ = 2.006, 2.006, and 2.0045). At this temperature, the shape of the EPR spectra is marked by symmetrical shoulders, which are created by hyperfine coupling between the nitrogen nuclei and the thermally activated unpaired electrons. With an increase in the time delay of heating at constant temperature or alternatively an increase of the temperature, a drastic enhancement is noticed for the EPR signal. In parallel, the EPR line becomes sharp without any resolved details from hyperfine coupling. This behavior is clearly the mark of an increase in the mobility of unpaired electrons, which contribute to motional narrowing of the EPR line. The radical concentration is marked by a kinetic process with relaxation times on the order of 15−60 min depending on the heating

DOI: 10.1021/acs.inorgchem.5b00975
Inorg. Chem. 2015, 54, 8923−8930

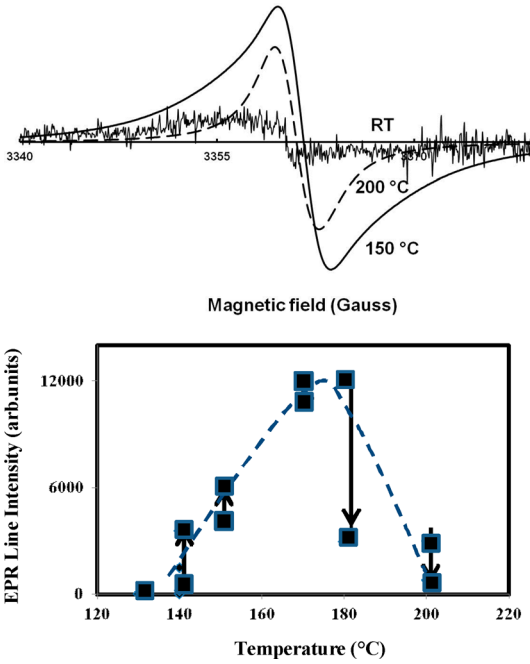

Figure 6. EPR spectra at different heating temperatures (top) and line-intensity evolution versus temperatures and kinetic time delays (140 °C, 60 min; 180 °C, 15 min; 200 °C, 30 min).

temperature. The maximum of the radical concentration is observed at 180 °C. Then, a rapid decrease occurs over this temperature, leading to only residual concentration (Figure 6).

If the dark-green crystals heated at 180 °C are rapidly cooled, the initial yellow-brown color is recovered after a few hours at room temperature, as in the case of the photochromic behavior at room temperature. A very nice and interesting feature is the regular discoloration of crystals from the "edge" to the "core" (Figure 5c). Except recently for a PCP compound containing methylviologen cations in pores where a rough edge to core discoloration was observed,[28] there was no report of such nice discoloration among the photo- or thermochromic compounds based on bipyridinium and carboxylate or chloride entities, certainly because of the dense nature of these hybrids. Because of the porous nature of **3**, the discoloration, which is due to a reoxidation of viologen entities, very certainly follows the diffusion of O_2 inside the pores. In fact, we could qualitatively check that the discoloration is slower when the atmosphere is poorer in O_2. Finally, such crystals could be used as O_2 sensors, with the discolored domain being related to the pressure of O_2 and the time of exposure to O_2. Crystals previously rapidly heated to 180 °C and cooled promptly, which have recovered their initial color at room temperature, can change their color again under the light of the microscope (photochromism) or again upon heating (thermochromism), and this can be repeated for a lot of cycles, without detectable loss of efficiency of the color change. Thus, the photo- and thermochromic processes are observed for both the solvated as-synthesized compound and the partially desolvated crystals (crystals heated at 180 °C and cooled rapidly did not lose all DMF solvent molecules). This feature certainly means that these processes are not really influenced by the presence of solvent in the pores, unfortunately. In fact, the solvent-dependent photo- or thermochromic properties could be an interesting transduction scheme in such systems. An explanation of the different optical properties, photochromism of **3**, or absence of photo- or thermochomism in **3′** may be advanced through close examination of intermolecular interactions involving bipyridinium acceptor units. Two independent hpc1 molecules are found in the asymmetric unit of **3**. For the first one, the bipyridinium core is sandwiched between two BDC^{2-} anions, with the shorter $N^+\cdots C(BDC^{2-})$ contact of 3.584(6) Å (see the SI) meaning that pyridinium units are not accessible to guest molecules, while such a situation is not known to lead to the PICT process. More interesting is the second hpc1 molecule, which is located at the border of the pores, being accessible. Nevertheless, because of a short interaction with a oxygen atom of a neighboring BDC^{2-} anion [d(N2···O9)= 3.441(3) Å; Figure 7a], the pyridinium cycle is rotated along the molecular

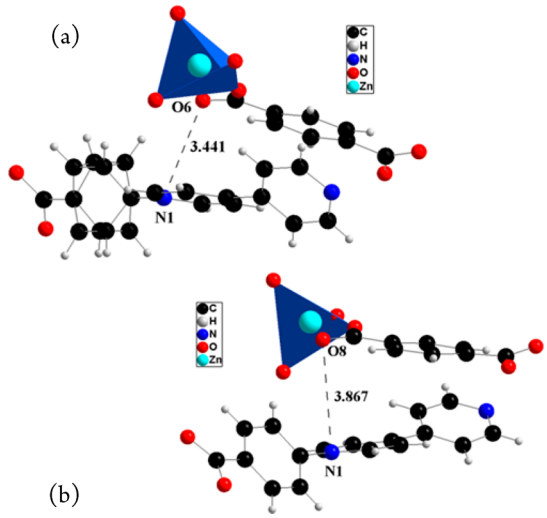

Figure 7. Interactions involving the pyridinium unit in the structure of **3** (a) and in the structure of the corresponding desolvated compound **3′** (b).

long axis so that the N^+ site cannot be directly involved in contacts with guest molecules. Such a short donor−acceptor contact between the carboxylate and pyridinium units is, as is known, favorable to the PICT process[14,15] and is very certainly responsible for the photochromic properties of **3** and the thermochromic properties as well. Through the irreversible transformation of **3** to the high-temperature-phase **3′**, the relative disposition of the two partners is modified in such a way that the shorter $N^+\cdots O(BDC^{2-})$ contact is increased to 3.867(6) Å. Such a distance is out of the range of common $N^+\cdots O$ distances observed in photochromic materials, and as a consequence, **3′** is, in fact, not photo- and thermochromic.

3.3. Adsorption Properties of 1, 2, and 3′. The prepared solids do not adsorb N_2 at liquid-nitrogen temperature (−196 °C). To verify the presence of open pores in such a case, other probe molecules can be used, e.g., CO_2[29] or MeOH.[7] Adsorption of the latter at 25 °C was used in our study. The obtained isotherms (Figure 8) show that all samples possess open pores, with sample **2** adsorbing the highest amount of MeOH in accordance with its most open structure. Given that the CH_3OH and N_2 molecules are similar in size (3.60 and 3.64 Å, respectively), the absence of any adsorption of N_2 can thus be attributed to kinetic effects or to pore shrinkage at low temperature due to framework flexibility. It can be seen from Figure 8 that for all samples the isotherms exhibit a large hysteresis; i.e., the desorption branch does not coincide with the adsorption one in a wide pressure range. This feature is

DOI: 10.1021/acs.inorgchem.5b00975
Inorg. Chem. 2015, 54, 8923−8930

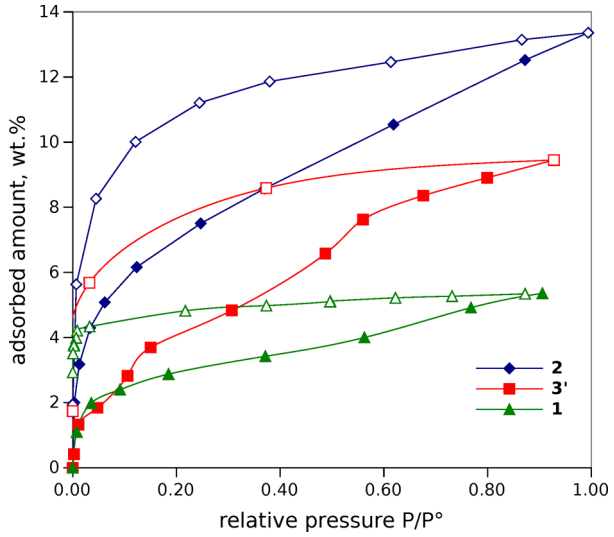

Figure 8. MeOH adsorption isotherms of **1**, **2**, and **3′** measured at 25 °C (closed symbols, adsorption; open symbols, desorption).

frequently observed in PCPs, and it is generally attributed to the flexible nature of the framework (the so-called "gate effect").[30−33] This is also the case for MeOH adsorbed in the viologen-containing PCPs reported by Kitagawa et al.[7] It is worth noting, however, that, in contrast to Kitagawa's compound, in our materials the hysteresis loops do not close at 25 °C (Figure 8). Even after a prolonged treatment under vacuum (for 48 h), a measurable amount of MeOH is retained in the pores (2.9, 1.9, and 1.7 wt % or 0.92, 0.59, and 0.54 mmol g^{-1} for **1**, **2**, and **3′** correspondingly). The residual MeOH can be completely desorbed only upon heating under vacuum at 170 °C. Such a behavior shows that some MeOH molecules interact with the pore walls much more strongly than others. The charge-transfer interaction with viologen species is very certainly the origin of this strong interaction. In fact, we can notice that the amount of MeOH retained in the pores of **1** and **3′** (0.92 and 0.54 mmol g^{-1}, respectively) corresponds approximately to the quantity of accessible bipyridinium moieties: 1.09 mmol g^{-1} in **1** and half of the bipyridinium units (1.24/2 = 0.62 mmol g^{-1}) in **3′** (see the structure description). In the case of compound **2**, the amount of MeOH retained in the pores (0.59 mmol g^{-1}) is quite smaller than the quantity of accessible bipyridinium moieties (0.99 mmol g^{-1}).

3.4. Conclusion. In conclusion, three new rare PCPs based on bipyridinium carboxylate ligands have been synthesized. A challenge using such ligands for the building of porous materials is the accessibility of pyridinium cycles to guest molecules because these redox units have a great tendency to interact with electron-rich sites of the host, either oxygen atoms of the carboxylate groups or electron-rich aromatic rings. In the best case, one side of the pyridinium cycle is accessible, as in the structure of **1**. When pyridinium rings are at the border of the pores, even if N^+···guest contacts are difficult, as in the structure of **3**, the presence of a local dipolar moment in the walls due to the presence of "CO_2^-···N^+" units has a positive impact on the detection or storage of polar guest molecules. This is highlighted in this work by the MeOH adsorption properties of **1**, **2**, and **3′**. Upon irradiation, **1** and **3** exhibit a color change from light brown to dark green because of the presence of bipyridinium radicals, resulting from electron transfer from the electron-donor carboxylate groups to the electron-acceptor pyridinium cycles. Particularly, crystals of **3**, which are very photosensitive, giving an eye-detectable color change upon exposure to the light of the microscope in air within 1−2 min, are also thermochromic. A very nice and interesting feature is the regular discoloration of crystals of **3** from the "edge" to the "core" upon exposure to O_2 (reoxidation of organic radicals) very certainly due to the diffusion of O_2 inside the pores, with this discoloration being slower in an O_2-poor atmosphere. It must be noted that the photo- or thermochromic processes seem not to be influenced by the presence of solvent, unfortunately. In fact, such solvent-dependent photo- or thermochromic properties could be an interesting transduction scheme in such systems. Works in this direction are in progress.

■ ASSOCIATED CONTENT

Supporting Information

The Supporting Information is available free of charge on the ACS Publications website at DOI: 10.1021/acs.inorgchem.5b00975.

Synthetic procedures, single-crystal data, PXRD patterns, thermodiffractometry, TGA, EPR spectrum of irradiated crystals of **3** (PDF)

Single-crystal crystallographic data in CIF format (CIF)

■ AUTHOR INFORMATION

Corresponding Author

*E-mail: nicolas.mercier@univ-angers.fr. Tel: 33.2.41.73.50.83.

Author Contributions

The manuscript was written through contributions of all authors.

Notes

The authors declare no competing financial interest.

■ REFERENCES

(1) Special issue Metal Organic Frameworks: *Chem. Soc. Rev.* **2012**, *112*, 673−1268.

(2) (a) Suh, M. P.; Park, H. J.; Prasad, T. K.; Lim, D.-W. *Chem. Rev.* **2012**, *112*, 782−835. (b) Collins, D. J.; Zhou, H.-C. *J. Mater. Chem.* **2007**, *17*, 3154. (c) Rowsell, J. L. C.; Yaghi, O. M. *Angew. Chem., Int. Ed.* **2005**, *44*, 4670.

(3) Sumida, K.; Rogow, D. L.; Mason, J. A.; McDonald, T. M.; Bloch, E. D.; Herm, Z. R.; Bae, T.-H.; Long, J. R. *Chem. Rev.* **2012**, *112*, 724−781.

(4) Cheon, Y. E.; Suh, M. P. *Chem. Commun.* **2009**, *45*, 2296.

(5) (a) Suh, M. P.; Cheon, Y. E.; Lee, E. Y. *Coord. Chem. Rev.* **2008**, *252*, 1007. (b) Farha, O. K.; Shultz, A. M.; Sarjeant, A. A.; Nguyen, S. T.; Hupp, J. T. *J. Am. Chem. Soc.* **2011**, *133*, 5652. (c) Shultz, A. M.; Sarjeant, A. A.; Farha, O. K.; Hupp, J. T.; Nguyen, S. T. *J. Am. Chem. Soc.* **2011**, *133*, 13252−13255.

(6) (a) Mulfort, K. L.; Farha, O. K.; Stern, C. L.; Sarjeant, A. A.; Hupp, J. T. *J. Am. Chem. Soc.* **2009**, *131*, 3866. (b) Nouar, F.; Eckert, J.; Eubank, J. F.; Forster, P.; Eddaoudi, M. *J. Am. Chem. Soc.* **2009**, *131*, 2864.

(7) Higuchi, M.; Tanaka, D.; Horike, S.; Sakamoto, H.; Nakamura, K.; Takashima, Y.; Hijikata, Y.; Yanai, N.; Kim, J.; Kato, K.; Kubota, Y.; Takata, M.; Kitagawa, S. *J. Am. Chem. Soc.* **2009**, *131*, 10336−10337.

(8) (a) Yao, Q.-X.; Pan, L.; Jin, X.-H.; Li, J.; Ju, Z.-F.; Zhang, J. *Chem. - Eur. J.* **2009**, *15*, 11890−11897. (b) Tan, B.; Chen, C.; Cai, L.-X.; Zhang, Y.-J.; Huang, X.-Y.; Zhang, J. *Inorg. Chem.* **2015**, *54*, 3456.

(9) (a) Kanoo, P.; Matsuda, R.; Sato, H.; Li, L.; Jeon, H. J.; Kitagawa, S. *Inorg. Chem.* **2013**, *52*, 10735−10737. (b) Lin, J.-B; Shimizu, G. K. H. *Inorg. Chem. Front.* **2014**, *1*, 302.

DOI: 10.1021/acs.inorgchem.5b00975
Inorg. Chem. 2015, 54, 8923−8930

(10) Aulakh, D.; Varghese, J. R.; Wriedt, M. *Inorg. Chem.* **2015**, *54*, 1756−1764.
(11) (a) Sen, S.; Yamada, T.; Kitagawa, H.; Bharadwaj, P. K. *Cryst. Growth Des.* **2014**, *14*, 1240−1244. (b) Lalonde, M. B.; Getman, R. B.; Lee, J. Y.; Roberts, J. M.; Sarjeant, A. A.; Scheidt, K. A.; Georgiev, P. A.; Embs, J. P.; Eckert, J.; Farha, O. K.; Snurr, R. Q.; Hupp, J. T. *CrystEngComm* **2013**, *15*, 9408−9414.
(12) Monk, P. M. S. *The Viologens: Physicochemical Properties, Synthesis, and Application of the Salt of 4,4′-Bipyridine*; Wiley: New York, 1998.
(13) (a) Prout, C. K.; Wright, J. D. *Angew. Chem., Int. Ed. Engl.* **1968**, *7*, 659. (b) Macfarlane, A. J.; Williams, J. P. *J. Chem. Soc. A* **1969**, 1517.
(14) (a) Mercier, N. *Eur. J. Inorg. Chem.* **2013**, *2013*, 19−31. (b) Leblanc, N.; Bi, W.; Mercier, N.; Auban-Senzier, P.; Pasquier, C. *Inorg. Chem.* **2010**, *49*, 5824. (c) Leblanc, N.; Allain, M.; Mercier, N.; Sanguinet, L. *Cryst. Growth Des.* **2011**, *11*, 2064−2069.
(15) Wang, M.-S.; Xu, G.; Zhang, Z.-J.; Guo, G.-C. *Chem. Commun.* **2010**, *46*, 361.
(16) Yao, Q. X.; Ju, Z. F.; Jin, X. H.; Zhang, J. *Inorg. Chem.* **2009**, *48*, 1266−1268.
(17) Sun, J.-K.; Wang, P.; Chen, C.; Zhou, X.-J.; Wu, L.-M.; Zhang, Y.-F.; Zhang, J. *Dalton Trans.* **2012**, *41*, 13441−13446.
(18) Sun, J.-K.; Wang, P.; Yao, Q.-X.; Chen, Y.-J.; Li, Z.-H.; Zhang, Y.-F.; Wu, L.-M.; Zhang, J. *J. Mater. Chem.* **2012**, *22*, 12212−12219.
(19) Sun, J.-K.; Jin, X.-H.; Cai, L.-X.; Zhang, J. *J. Mater. Chem.* **2011**, *21*, 17667−17672.
(20) Sun, Y.-Q.; Zhang, J.; Ju, Z.-F.; Yang, G.-Y. *Cryst. Growth Des.* **2005**, *5*, 1939−1943.
(21) Jin, X.-H.; Sun, J.-K.; Xu, X.-M.; Li, Z.-H.; Zhang, J. *Chem. Commun.* **2010**, *46*, 4695−4697.
(22) Li, H.-Y.; Wei, Y.-L.; Dong, X.-Y.; Zang, S.-Q.; Mak, T. C. *Chem. Mater.* **2015**, *27*, 1327−1331.
(23) Kreno, L. E.; Leong, K.; Farha, O. K.; Allendorf, M.; Van Duyne, R. P.; Hupp, J. T. *Chem. Rev.* **2012**, *112*, 1105−1125.
(24) (a) Lin, X.; Blake, A. J.; Wilson, C.; Sun, X. Z.; Champness, N. R.; George, M. W.; Hubberstey, P.; Mokaya, R.; Schröder, M. *J. Am. Chem. Soc.* **2006**, *128*, 10745. (b) Hinks, N. J.; McKinlay, A. C.; Xiao, B.; Wheatley, P. S.; Morris, R. E. *Microporous Mesoporous Mater.* **2010**, *129*, 330−334.
(25) Kosaka, W.; Yamagishi, K.; Hori, A.; Sato, H.; Matsuda, R.; Kitagawa, S.; Takata, M.; Miyasaka, H. *J. Am. Chem. Soc.* **2013**, *135*, 18469.
(26) Han, L.; Qin, L.; Xu, L. P.; Zhao, W. N. *Inorg. Chem.* **2013**, *52*, 1667.
(27) Shimomura, S.; Matsuda, R.; Tsujino, T.; Kawamura, T.; Kitagawa, S. *J. Am. Chem. Soc.* **2006**, *128*, 16416.
(28) Gong, Y.-N.; Lu, T.-B. *Chem. Commun.* **2013**, *49*, 7711−7713.
(29) Bhunia, A.; Boldog, I.; Möller, A.; Janiak, C. *J. Mater. Chem. A* **2013**, *1*, 14990−14999.
(30) Mondal, S. S.; Bhunia, A.; Kelling, A.; Schilde, U.; Janiak, C.; Holdt, H.-J. *Chem. Commun.* **2014**, *50*, 5441−5443.
(31) Mondal, S. S.; Bhunia, A.; Kelling, A.; Schilde, U.; Janiak, C.; Holdt, H.-J. *J. Am. Chem. Soc.* **2014**, *136*, 44−47.
(32) Mondal, S. S.; Dey, S.; Baburin, I. A.; Kelling, A.; Schilde, U.; Seifert, G.; Janiak, C.; Holdt, H.-J. *CrystEngComm* **2013**, *15*, 9394−9399.
(33) Mondal, S. S.; Bhunia, A.; Baburin, I. A.; Jäger, C.; Kelling, A.; Schilde, U.; Janiak, C.; Holdt, H.-J. *Chem. Commun.* **2013**, *49*, 7567−7570.

DOI: 10.1021/acs.inorgchem.5b00975
Inorg. Chem. 2015, 54, 8923−8930